CHEMISTRY
A EUROPEAN JOURNAL

FULL PAPER

DOI: 10.1002/chem.201300872

VIP

Transition Metal Complexes of a Salen–Fullerene Diad: Redox and Catalytically Active Nanostructures for Delivery of Metals in Nanotubes

Maria A. Lebedeva, Thomas W. Chamberlain, E. Stephen Davies, Dorothée Mancel, Bradley E. Thomas, Mikhail Suyetin, Elena Bichoutskaia, Martin Schröder,* and Andrei N. Khlobystov*[a]

Dedicated to Professor Maurizio Prato on the occasion of his C60th birthday

Abstract: A covalently-linked salen–C_{60} (H_2L) assembly binds a range of transition metal cations in close proximity to the fullerene cage to give complexes [M(L)] (M = Mn, Co, Ni, Cu, Zn, Pd), [MCl(L)] (M = Cr, Fe) and [V(O)L]. Attaching salen covalently to the C_{60} cage only marginally slows down metal binding at the salen functionality compared to metal binding to free salen. Coordination of metal cations to salen–C_{60} introduces to these fullerene derivatives strong absorption bands across the visible spectrum from 400 to 630 nm, the optical features of which are controlled by the nature of the transition metal. The redox properties of the metal–salen–C_{60} complexes are determined both by the fullerene and by the nature of the transition metal, enabling the generation of a wide range of fullerene-containing charged species, some of which possess two or more unpaired electrons. The presence of the fullerene cage enhances the affinity of these complexes for carbon nanostructures, such as single-, double- and multiwalled carbon nanotubes and graphitised carbon nanofibres, without detrimental effects on the catalytic activity of the metal centre, as demonstrated in styrene oxidation catalysed by [Cu(L)]. This approach shows promise for applications of salen–C_{60} complexes in heterogeneous catalysis.

Keywords: carbon nanotubes · catalysis · fullerenes · salen · transition metals

Introduction

Fullerenes and their derivatives possess redox and optical properties that make them ideal components in systems for photoactivation, such as photovoltaics and photocatalysis.[1–3] Transition-metal complexes also provide a wealth of redox, optical and magnetic properties, and the combination of fullerene with bound transition metal ions can be utilised to form molecular or supramolecular systems with tunable physicochemical properties. This represents an important step towards the development of molecular electronic devices for data storage, molecular machines,[4] molecular switches, sensors, photoconductors and photoactive dyads as well as the next generation of light activated catalysts.[5] The desire to fabricate such systems has led to the development of several classes of fullerene and metal containing compounds. These include endohedral fullerenes,[6] in which metal atoms are trapped inside the fullerene cage, and various solid-state co-crystallites[7] and charge-transfer systems,[8] in which the fullerene cage and the metal are held together by electrostatic or other intermolecular interactions. Transition-metal complexes, where the transition metal atoms are bonded to the outside of the fullerene,[9] and so-called metalated bucky-ligands, in which a metalated ligand is covalently attached to the fullerene cage, are also important targets.

The synthesis of fullerene derivatives containing metal binding groups has received significant attention,[10] due in part to the molecular nature of the species formed in which the metal atoms are bound in discrete coordination environments. A large variety of ligand moieties have been attached to C_{60}, including macrocycles, such as porphyrins,[11] phthalocyanines,[12] and crown ethers[13] and tri-, bi- and monodentate metal binding groups, such as terpyridines, bipyridines,[14] and dipyrrins,[15] and pyridines.[16] However, the rapid advancement of this area has been hindered by difficulties in the synthesis of functionalised fullerene ligands or the poor solubility of the resultant metal complexes. Therefore, no "universal" {fullerene}–{metal binding group} combination has yet been identified that can coordinate a wide variety of metal centres.

We report herein the synthesis of a new {metal receptor}–C_{60} dyad assembly incorporating the tetradentate N_2O_2-coordinating Schiff-base ligand salen (*N*,*N*′-ethylenebis(salicylimine)). We demonstrate that the salen moiety in this system

[a] M. A. Lebedeva, Dr. T. W. Chamberlain, Dr. E. S. Davies, Dr. D. Mancel, B. E. Thomas, Dr. M. Suyetin, Dr. E. Bichoutskaia, Prof. Dr. M. Schröder, Prof. Dr. A. N. Khlobystov
School of Chemistry, University of Nottingham
Nottingham NG7 2RD (UK)
E-mail: M.Schroder@nottingham.ac.uk
Andrei.Khlobystov@nottingham.ac.uk

Supporting information for this article is available on the WWW under http://dx.doi.org/10.1002/chem.201300872.

can bind to a wide range of transition metal cations ({^{IV}V(O)}, Cr^{III}, Mn^{II}, Fe^{III}, Co^{II}, Ni^{II}, Cu^{II}, Zn^{II} and Pd^{II}) to form stable and soluble metal complexes. The introduction of redox-active metal centres enables fine-tuning of the electron-acceptor properties of the salen–C_{60} compounds and significantly broadens the range of available reduced states, which are both important for the application of fullerenes in photovoltaics and electrocatalysis. Furthermore, many of the reduced species possess two or more unpaired electrons presenting an opportunity for the exploitation of the electrochemically controlled magnetic states of salen–C_{60} complexes in quantum information processing and molecular spintronic devices. M(salen)–C_{60} complexes exhibit catalytic activity in reactions of (ep)oxidation, characteristic of metal–salen complexes.[17] The presence of a fullerene cage bound to a metal–salen moiety does not hinder catalysis but facilitates the deposition of these catalytic centres onto a variety of carbon-based support materials offering a new methodology for engineering catalytically active surfaces at nanoscale.

Results and Discussion

Ligand synthesis: We have developed a five-step procedure for the synthesis of a salen–C_{60} metal receptor, **5**, which incorporates a salen metal binding moiety and a C_{60} cage covalently linked via a cyclohexenyl bridge (Scheme 1). Four *tert*-butyl groups were introduced into the aromatic backbone to provide solubility to **5** and its corresponding metal complexes. Complexes of the corresponding salen–C_{60} systems not incorporating *tert*-butyl groups were found to be only very sparingly soluble.

The synthesis of **5** (H_2L) began with protection of 4,5-*o*-phenylene diamine with a *tert*-butyloxycarbonyl (Boc) group[18] to give **1** in 80% yield. Subsequent bromination with *N*-bromosuccinimide (NBS) in the presence of benzoyl peroxide in CCl_4[19] gave the bis(bromomethyl) derivative **2** in 20% yield. Compound **2** was treated with C_{60} fullerene in the presence of KI and 18-crown-6 in dry toluene[20] to give the Diels–Alder cycloaddition product **3** in 20% yield. Deprotection of the amine groups in **3** was achieved using a large excess of TFA (10 equiv) in $CHCl_3$ to give **4** (65% yield). The diamine **4**, which decomposes gradually over a few days, was purified by column chromatography and characterised spectroscopically. Condensation of freshly prepared **4** and 3,5-di-*tert*-butyl salicylic aldehyde was carried out in the presence of a catalytic amount of TFA in tetrahydrofuran (THF) instead of the more commonly used alcoholic solvents[21] in order to improve the solubility of the fullerene precursor. Mixtures of compounds **4** and **5** cannot be readily separated and so the conversion of **4** to **5** was performed with a significant excess of aldehyde to ensure full conversion of the diamine (monitored by TLC and MALDI MS). Any aldehyde present after the reaction was conveniently removed from the product material by washing with methanol (MeOH).

Metal complex formation: The efficacy of **5** to bind a range of metal centres was investigated. The general procedure involved the heating of **5** and a metal salt as a solution in a 10:1 v/v mixture of THF/MeOH under reflux. The majority of the metal precursors utilised were M^{II} salts (M = Mn, Co, Ni, Cu, Zn, Pd) or {^{IV}V(O)}, which formed neutral metal–salen complexes upon complexation. For MCl_3 salts (M = Cr and Fe), treatment with **5** resulted in the formation of metal–salen complexes having an additional chloride ligand bound to the metal (Scheme 1). For V(O), Cu and Ni, the rate of metal complex formation was significantly increased in the presence of triethyl amine as a base.[22] Complexes **6**–**12** and **14** were found to be highly soluble in solvents typically used for solubilising fullerenes (CS_2, *o*-dichlorobenzene (ODCB)) and displayed moderate solubility in common organic solvents, such as $CHCl_3$, CH_2Cl_2, and THF. In contrast the Zn complex, **13**, was found to be insoluble in all solvents including DMF and pyridine, consistent with other Zn^{II}–salen systems; this is attributed to the formation of Zn–O–Zn bonds between two or more molecules,

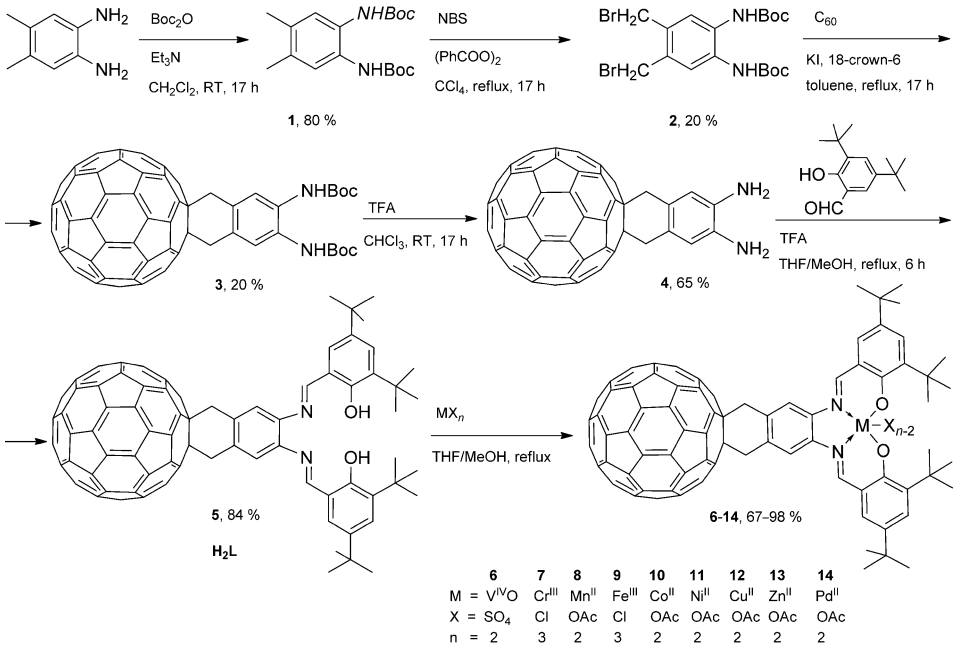

Scheme 1. Synthesis of the fullerene–salen ligand, **5**, and corresponding metal complexes **6**–**14**.

which drastically reduces the solubility of the complex.[23,24] MALDI-TOF MS for each of the complexes **6**–**14** shows a molecular ion and peak distribution entirely consistent with theoretical predictions and confirms the presence of 1:1 metal/ligand stoichiometries in all cases (see the Supporting Information). The resultant complexes were found to be stable under ambient conditions in air, with the exception of the Mn complex, **8**, which was observed to oxidise partially to Mn^{III} in air forming an oxo-bridged binuclear complex [(Salen)Mn–O–Mn(Salen)] as confirmed by MALDI-TOF MS and CV measurements (see the Supporting Information).

Metal complex formation with salen–C_{60} (H_2L) is accompanied by a change in the colour of the reaction mixture. Therefore, the kinetics of the metal coordination process can be conveniently followed by UV/Vis absorption spectroscopy. Additionally, for diamagnetic compounds, such as the Pd (**14**) and Ni (**11**) complexes, ^{1}H NMR spectroscopy can be used to monitor complex formation by observing the loss of the OH signal of the free ligand, H_2L, at 13.42 ppm, the shifts of the imine proton signal at 8.84 ppm in H_2L to lower values (8.36 ppm for [Ni(L)], 8.70 ppm for [Pd(L)] and the shifts of the aromatic ring signals from 7.57 and 7.39 ppm in H_2L to higher values (8.19 and 7.53 ppm in [Pd(L)], and 8.00 and 7.38 ppm in [Ni(L)], respectively). Infrared spectroscopy can also confirm the deprotonation of the salen moiety through the loss of ν(O–H) at 3445 cm^{-1} in all metal complexes. However, the C=N bond stretch observed between 1615–1620 cm^{-1} experiences only a minor shift in complexes **6**–**14** as compared to the free ligand H_2L (see the Experimental Section).

Metal binding studies: To quantify the kinetics of complexation, the coordination of Co, Ni, Cu and Pd cations to H_2L was investigated in detail. These data were compared to those obtained for metal complexation to a reference salen ligand with identical structure but not attached to C_{60} (compound **15** (H_2L'), Scheme 2) in order to evaluate the influence of the fullerene moiety on the ability of the salen to bind metals. Reactions between $Co(OAc)_2$, $Ni(OAc)_2$, and $Cu(OAc)_2$ and H_2L and H_2L' were monitored by UV/Vis spectroscopy in THF, and between $Pd(OAc)_2$ and the same ligands by ^{1}H NMR spectroscopy in deuterated THF.

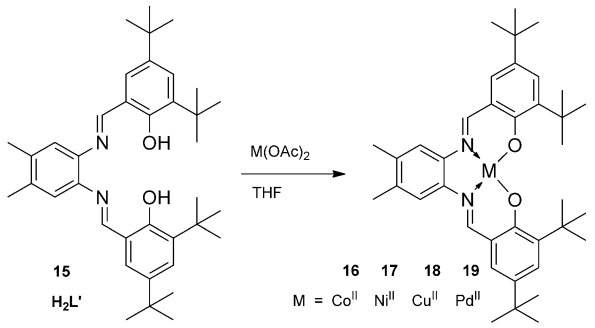

Scheme 2. Synthesis of complexes of a reference salen ligand without fullerene **15** (H_2L').

The reaction between the metal salts and H_2L can be represented by:

$$H_2L + MX_2 = ML + 2\,HX \quad (1)$$

in which X is anion. The salts $M(OAc)_2$ (M = Co, Ni, Cu) are six-coordinate, octahedral complexes in solution with the metal centres bound by either four oxygen atoms of two bidentate carboxylates and two solvent molecules in axial positions as in the case of $Cu(OAc)_2$,[25] or by two oxygen atoms of two monodentate carboxylates and four solvent molecules as found for $Ni(OAc)_2$[26] and $Co(OAc)_2$.[21,27] In contrast, $Pd(OAc)_2$ exists as discrete trimers in solution[28] with the metal centre strongly bound to four equatorially coordinated acetate oxygen atoms and two weakly coordinated molecules of solvent in the axial positions. Therefore, Equation (1) can be treated as ligand substitution of an octahedral complex according to the Eigen–Wilkins mechanism (Scheme 3).

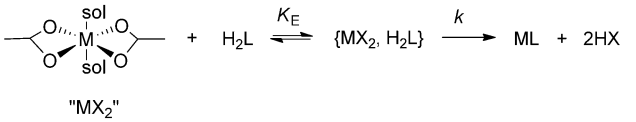

Scheme 3. The Eigen–Wilkins mechanism for the substitution of an acetate ligand by H_2L at M^{II} (M = Co, Ni, Cu, Pd).

Within the framework of the Eigen–Wilkins formalism (for details see the Supporting Information) the observed rate constants (k_{obs}) have been measured for each complex formation at three different temperatures and subsequently the activation energies (E_a) for complex formation were determined from the Arrhenius equation for Co, Ni, Cu and Pd complexes (Table 1, Table 2).

Figure 1 and Figure 2 summarise the analyses for complex formation as measured by UV/Vis and ^{1}H NMR spectroscopy (see the Supporting Information for the control experiments). Comparisons of the formation of complexes [M(L)] and [M(L′)] (M = Co, Ni, Cu, Pd; Tables 1 and 2) confirms that the presence of the C_{60} fullerene moiety slows down metal binding by 5–15 %, corresponding to a 10–20 kJ mol^{-1} increase in the activation barrier. The higher activation barriers observed for complexation reactions for H_2L can be related to an increase in steric bulk of the ligand, which inhibits the approach to the metal acetate molecule during the initial stage of complex formation, or the electron withdrawing (inductive) effect of the fullerene cage on the salen moiety.

DFT geometry optimisation of the complexes [M(L)] confirms that the salen group binds to the metal centres in a square plane as observed in conventional metal–salen complexes that do not incorporate the fullerene (Figure 3a).[29] The donor atoms are arranged in a slightly distorted square planar geometry around the Ni centre with bond angles deviating only marginally from 90° (Table 3). The cyclohexenyl ring, which links salen and C_{60} moieties, adopts a boat-like

Table 1. Observed rate constants k_{obs} [s^{-1} м$^{-1}$] activation energies E_a [kJ mol^{-1}] and ln(A·K_E) parameters for formation of [M(L)] and [M(L′)] (M = Cu, Co, Ni) determined by UV/Vis spectroscopy at various temperatures [°C].

Parameter	T [°C]	H_2L+Co^{II}	$H_2L'+Co^{II}$	T [°C]	H_2L+Ni^{II}	$H_2L'+Ni^{II}$	T [°C]	H_2L+Cu^{II}	$H_2L'+Cu^{II}$
k_{obs}	25	0.369± 0.003	0.625± 0.003	30	0.024± 0.002	0.0249± 0.0003	25	1.485± 0.007	1.960± 0.009
	35	1.292± 0.009	1.327± 0.051	40	0.0549± 0.0002	0.0719± 0.0004	30	2.526± 0.008	2.875± 0.013
	40	2.042± 0.019	2.501± 0.010	50	0.1389± 0.0001	0.1114± 0.0040	35	3.632± 0.013	3.905± 0.006
E_a		89.5±2.7	69.1±0.3		70.7±0.3	61.1±1.0		67.7±0.2	53.2±0.3
ln(A·K_E)		35.1	27.4		24.3	20.6		27.7	22.1

Table 2. Observed rate constants k_{obs} [s^{-1} м$^{-1}$] activation energies E_a [kJ mol^{-1}] and ln(A·K_E) parameters for [Pd(L)] and [Pd(L′)] determined by ^{1}H NMR spectroscopy at various temperatures [°C].

Parameter	T [°C]	H_2L+Pd^{II}	$H_2L'+Pd^{II}$
$k_{obs}\times10^3$	45	1.651±0.031	1.994±0.041
	55	3.572±0.071	3.989±0.100
	65	6.273±0.151	6.300±0.204
E_a		59.7±0.2	51.5±0.5
ln(A·K_E)		25.6	13.3

conformation providing an angle of 124° between the plane defined by [Ni(salen)] and the fullerene cage (Figure 3b). Despite the angular conformation of the cyclohexenyl connection, the metal centre is separated by about 6.7 Å from the fullerene, thus precluding any interactions between the d-orbitals of the metal centre and the π-system of the carbon cage. However, the proximity of the fullerene cage to the donor atoms of the salen group is likely to have some hindering effects on metal coordination, which is consistent with the kinetic measurements discussed above.

Optical and redox properties of metal complexes: H_2L exhibits two bands at 710 and 436 nm in the UV/Vis spectrum characteristic of a [6,6]-functionalised fullerene cage,[30] and strong bands at 300–430 nm associated with π–π* and n–π* transitions in the salen moiety.[31] Thus, the optical properties of H_2L can be viewed as a superposition of the individual fullerene and salen components. The coordination of a metal centre to L^{2-} results in the retention of absorption bands associated with the fullerene moiety, albeit with a shift to lower wavelengths compared to those of the free ligand. The optical transitions associated with the metal–salen centres appear between 366–630 nm, are metal dependent and in some complexes overlap with the bands of the fullerene moieties (Table 4).

The absorption bands for complexes **6**–**12** and **14** are assigned as either d–d transitions based on the metal centre, or d–π* charge transfer transitions from the metal to the ligand, typically with higher extinction coefficients for the latter. These data correlate well with other reported salen complexes[32–38] indicating that the electronic transitions based on the metal centres remain largely unperturbed by the presence of the fullerene cage. Although metal-to-ligand optical transitions dominate the UV/Vis absorption spectra of complexes **6**–**12** and **14**, no bands that could be assigned to metal-to-fullerene transitions were observed. All measurements indicate that the metal centre maintains a square planar or square-base pyramidal geometry in solution despite the close proximity of the fullerene group to the metal (Figure 3).

The transition metal centres also provide redox features, which in combination with the electron–acceptor properties of the fullerene cage form a basis for redox tuneable electron-spin active molecular systems. The electrochemical behaviours of compounds **5**–**12** and **14** have been investigated by cyclic and square-wave voltammetry at a glassy carbon electrode as ODCB solutions containing [NBu_4^+][BF_4^-] (0.2 м) as the supporting electrolyte (Table 5). The nature of the electron transfer for each redox process was assessed by monitoring the peak-to-peak separation and the ratio of peak currents at a range of scan rates between 0.02 and 0.3 Vs^{-1}. As a typical example the cyclic voltammogram of [Cu(L)] **12** is presented in Figure 4, and the results for all complexes are summarised in Table 5. These measurements confirm that the potentials of the three observed quasi-reversible reductions of the fullerene moiety are essentially unperturbed by variations of the metal centre and differ only slightly from those in the metal-free ligand H_2L (Table 5). These values are similar to others reported previously for fullerene derivatives.[39,40] Clearly, the large distance (6.7 Å) separating the metal centre of the salen moiety from the surface of the fullerene cage (Figure 3) and the lack of electronic conjugation between these centres is sufficient to preclude any electronic interactions between the metal and the fullerene.

In addition to the observed quasi-reversible fullerene-based reductions, metal centres contribute extra reduction processes. For example, **6** exhibits two quasi-reversible metal-related reductions for the $\{V(O)\}^{IV/III}$ and $\{V(O)\}^{III/II}$ processes at −1.43 and −1.66 V, respectively, but the $Co^{II/I}$ process in **10** at −1.30 V is essentially irreversible. Complexes **9** and **12** exhibit quasi-reversible reductions at −0.53 V $Fe^{III/II}$ and −1.36 V $Cu^{II/I}$, respectively. The reduction of the metal centres in **11** and **14** observed at −1.59 V $Ni^{II/I}$ and −1.56 V $Pd^{II/I}$, respectively, are also quasi-reversible. Since **8** is prone to oxidation in air during purification and storage, the process observed at −0.25 V was assigned to the $Mn^{III/II}$ reduction in an oxo-bridged binuclear complex [(L)Mn-O-Mn(L)], which forms over time as a result of partial oxidation in air, consistent with the results of MALDI MS for this complex (see the Experimental Section). The Cr^{III} complex **7** shows no metal-based reductions, which is consistent with the control complex [Cr(L′)Cl] and the fact that Cr^{II} is significantly less stable than Cr^{III}, so that reduction to Cr^{II} occurs at a much more negative potential, outside of the range of potentials studied. Thus, the choice of

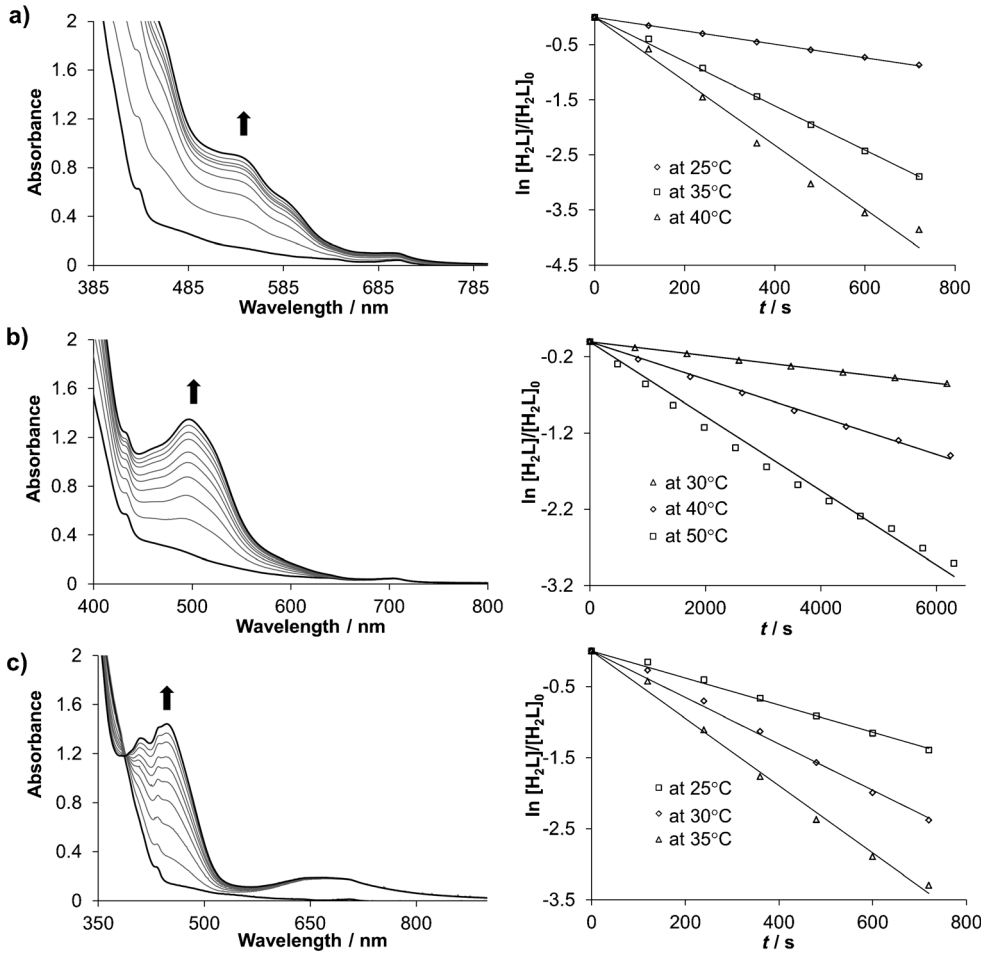

Figure 1. UV/Vis spectroscopic data for the titration of H_2L into MX_2 (left) and plots of $\ln[H_2L]/[H_2L]_0$ versus t used for the determination of the rate constant (right) for the formation of: a) [Co(L)], **10**, b) [Ni(L)], **11**, and c) [Cu(L)], **12**. Arrows in a)–c) (left) indicate the increase in concentration of [M(L)]; squares, triangles and diamonds and the corresponding temperature values describe the rate constants determination at different temperatures (right).

transition metal modifies the energy of the orbitals of the metal–salen moiety with respect to the fullerene thus tuning the electronic- and spin-states of the resultant fullerene/{metal–salen} adduct. Incorporation of transition metals Fe, Mn, Co, Ni, Cu, Pd or {V(O)} into H_2L increase the capacity of these fullerene derivatives for uptake of one or two electrons, in addition to the three electrons that can be reversibly deposited onto the fullerene cages in all studied complexes (Scheme 4).

All of the metal complexes **6**–**12** and **14** exhibit oxidation processes related to the formation of phenoxyl radicals on the salen moiety or oxidation of the metal centre (Table 6). For example, **6** and **10** show metal-based oxidations at +0.57 V $\{V(O)\}^{IV/V}$ and +0.74 V $Co^{II/III}$, respectively. Furthermore, the two *tert*-butyl groups on the phenol part of the ligand in the *ortho* and *para* positions are known to stabilise phenoxyl radicals,[41] which form in H_2L at +1.17 V. Metal coordination to H_2L stabilises the oxidised state of the salen moiety, thus lowering the potential for phenoxyl radicals formation to between +0.99 and +1.06 V.[42] Additionally, the Cr^{III}, Mn^{II}, Ni^{II} and Cu^{II} centres in complexes **7**, **8**, **11** and **12** promote the formation of a second phenoxyl radical in the salen as indicated by the oxidation potentials observed at +1.12, +1.41, +1.42 and +1.29 V, respectively. However, the presence of highly charged $\{V(O)\}^{V}$, Co^{III} and Fe^{III} centres inhibits oxidation of salen and shifts the potential of phenoxyl radicals formation to more anodic values (Scheme 4b).

Oxidation of the fullerene cage was not observed in our experiments.[43] Typically, oxidised fullerene species are difficult to access and have only limited stabilities, but the presence of the metal–salen group attached to the fullerene cage provides one or two reversible oxidations, some of which lead to the formation of electron-spin active species, without having to oxidise the fullerene cage (Scheme 4b). The ability to generate molecules with high total electron spin is desirable for molecular electronics and magnetic applications.[44]

Catalytic properties: Metal–salen compounds are known as catalysts for oxidation,[45] ring-opening of epoxides,[46] aldol condensation[47] and epoxidation[48] reactions. We have

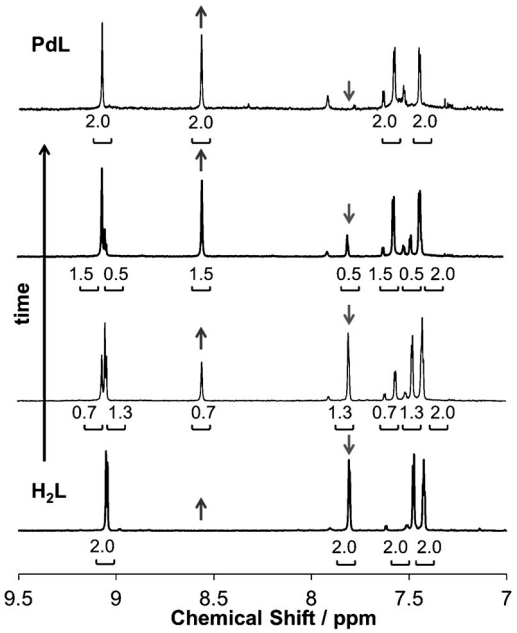

Figure 2. ^{1}H NMR spectroscopic data for the titration of H_2L into MX_2 showing an increase in the size of the aromatic H peak at 8.56 ppm of the complex [Pd(L)] and the decrease of the aromatic H peak at 7.81 ppm of the free ligand with complex formation.

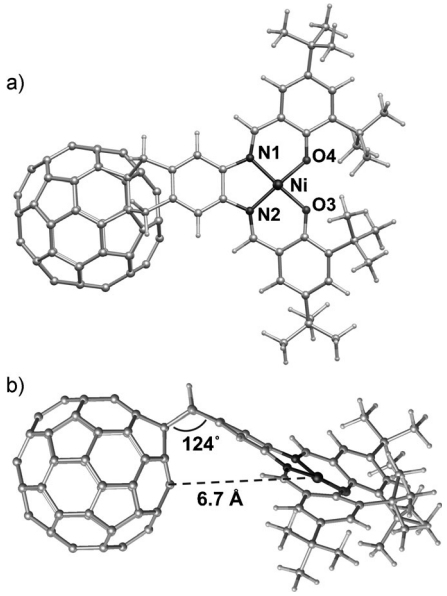

Figure 3. Calculated geometry of [Ni(L)], **11**, illustrating: a) the square planar geometry of the [Ni(salen)] moiety, and b) its position with respect to fullerene cage.

Table 3. Selected bond lengths [Å] and angles [°] of the [Ni(L)], **11**.

Length [Å]		Angle [°]	
Ni–N1	1.85	O3-Ni-O4	84.2
Ni–N2	1.84	O3-Ni-N2	95.0
Ni–O3	1.84	O4-Ni-N1	95.3
Ni–O4	1.84	N1-Ni-N2	86.3

Table 4. UV/Vis absorption bands for compounds **5**–**14** in CH_2Cl_2 solution.

Compound	UV/Vis, λ_{max} [nm] (ε [$\times 10^{-3}$ dm^3 mol^{-1} cm^{-1}])	
	fullerene moiety	metal–salen moiety
5	710 (0.413), 436 (6.587)	–
6	702 (0.31), 436 (14.87)	418 (14.68)
7	703 (0.31), 433 (4.20)	483 (4.36), 406 (4.45)
8	703 (0.68), 432 (7.32)	630 (1.06), 581 (1.68), 486 (6.97), 366 (20.18)
9	702 (0.65), 432 (11.54)	406 (13.66)
10	703 (0.729), 432 (15.555)	596 (3.784), 544 (6.655), 398 (25.184)
11	702 (0.20), 433 (4.98)	525 (4.35), 497 (5.43), 386 (15.28)
12	708 (0.62), 439 (22.88)	455 (23.53), 415 (21.92)
13	insoluble	insoluble
14	706 (1.478), 436 (12.153)	528 (9.885), 494 (10.882), 408 (16.819)

Table 5. Electrochemical data[a] for the reduction of compounds **5**–**12** and **14** (cyclic and square wave voltammograms are presented in the Supporting Information).

Compound	Fullerene reduction, $E_{1/2}$ [V] (ΔE [V])			Metal salen reduction, $E_{1/2}$ [V] (ΔE [V])		ΔE Fc^+/Fc [V][b]
	$E_{1/2}red_1$	$E_{1/2}red_2$	$E_{1/2}red_3$	$E_{1/2}red_4$	$E_{1/2}red_5$	
5	−0.61 (0.15)	−0.99 (0.17)	−1.52 (0.15)	–	–	0.14
6	−0.61 (0.15)	−1.00 (0.15)	−1.55 (0.13)	−1.43 (0.15)	−1.66	0.12
7	−0.60 (0.11)	−0.98 (0.10)	−1.52 (0.12)	–	–	0.11
8	−0.61 (0.10)	−0.98 (0.10)	−1.52 (0.10)	−0.25 (0.10)	–	0.07
9	−0.61 (0.15)	−1.00 (0.15)	−1.52	−0.53[b]	–	0.10
10	−0.61 (0.16)	−0.99 (0.16)	−1.55 (0.14)	−1.29 (0.17)	–	0.11
11	−0.61 (0.15)	−0.99 (0.15)	−1.53 (0.08)	−1.588 (0.09)	–	0.12
12	−0.62 (0.13)	−1.00 (0.15)	−1.55 (0.14)	−1.36 (0.16)	–	0.12
14	−0.61 (0.09)	−1.01 (0.10)	−1.52 (0.10)	−1.56 (0.09)	–	0.07

[a] Potentials ($E_{1/2}=(E_p^a+E_p^c)/2$) [V] quoted to the nearest 0.01 V. All potentials are reported against the $(\eta^5\text{-}Me_5C_5)_2Fe^+/(\eta^5\text{-}Me_5C_5)_2Fe$ couple for 0.5 mM solutions in ODCB containing 0.2 M [nBu$_4$N][BF$_4$] as the supporting electrolyte ($E_{1/2}$ ferrocene vs. $(\eta^5\text{-}Me_5C_5)_2Fe^+/(\eta^5\text{-}Me_5C_5)_2Fe = 0.52$ V). The anodic/cathodic peak separation ($\Delta E = E_p^a - E_p^c$) is given in brackets where applicable. [b] The ΔE for the $(\eta^5\text{-}Me_5C_5)_2Fe^+/(\eta^5\text{-}Me_5C_5)_2Fe$ couple used as the internal standard.

chosen oxidation of styrene with *tert*-butyl peroxide leading to benzaldehyde and styrene oxide as a model reaction to ascertain the influence of the fullerene cage on the catalytic properties of the metal centres. Cu-containing complex **12** demonstrates a catalytic activity comparable to fullerene-free Cu–salen complex, **18**, confirming that the addition of

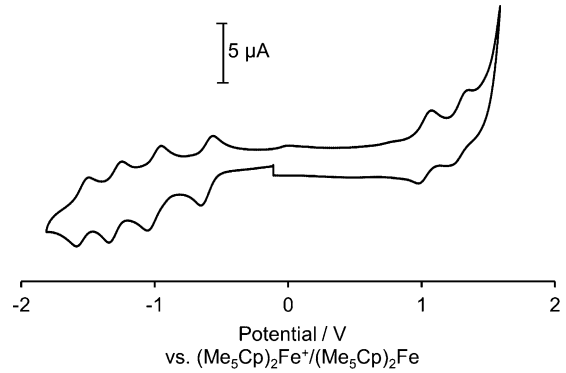

Figure 4. The cyclic voltammogram of **12** in ODCB with $[NBu_4^+][BF_4^-]$ (0.2 M) as supporting electrolyte at a scan rate of 0.1 Vs^{-1}.

Table 6. Electrochemical data[a] for the oxidation of compounds **5**–**12** and **14**. All potentials are quoted versus the $(Me_5Cp)_2Fe^+/(Me_5Cp)_2Fe$ couple (detailed electrochemical data are presented in the Supporting Information).

Compound	Metal oxidation $E_{1/2}$ [V] (ΔE [V]) $E_{1/2}ox_1$	Salen oxidation $E_{1/2}$ [V] (ΔE [V]) $E_{1/2}ox_2$	$E_{1/2}ox_3$	ΔE Fc^+/Fc [V][b]
5	–	1.17 (0.15)	–	0.14
6	0.57 (0.14)	–	–	0.12
7	–	1.06 (0.12)	1.12	0.11
8	–	1.18	1.41	0.07
9	–	1.31 (0.15)	–	0.10
10	0.74 (0.18)	1.30	–	0.11
11	–	0.99 (0.15)	1.42	0.12
12	–	1.03 (0.15)	1.29 (0.16)	0.12
14	–	1.05 (0.15)	–	0.07

[a] Potentials ($E_{1/2}=(E_p^a+E_p^c)/2$) [V] quoted to the nearest 0.01 V. All potentials are reported against the $(\eta^5\text{-}Me_5C_5)_2Fe^+/(\eta^5\text{-}Me_5C_5)_2Fe$ couple for 0.5 mM solutions in ODCB containing 0.2 M $[n Bu_4N][BF_4]$ as the supporting electrolyte ($E_{1/2}$ ferrocene vs. $(\eta^5\text{-}Me_5C_5)_2Fe^+/(\eta^5\text{-}Me_5C_5)_2Fe$ = 0.52 V). The anodic/cathodic peak separation ($\Delta E=E_p^a-E_p^c$) is given in brackets where applicable. [b] The ΔE for the $(\eta^5\text{-}Me_5C_5)_2Fe^+/(\eta^5\text{-}Me_5C_5)_2Fe$ couple used as the internal standard.

the fullerene cage does not have a detrimental effect on the activity of the metal centre (Figure 5). The electron withdrawing ability of fullerene depletes the electronic density at the catalytic centre in complex **12** and may be responsible for the slight increase in the observed catalytic activity of **12** as compared to the control compound **18**. However, the observed increase is small and only marginally greater than the error of these measurements (Figure 5).

The ability to anchor catalytic centres to solid supports is essential for the development of effective heterogeneous catalysts. Thus, salen has been supported on polymer beads,[49] zeolites,[50] and covalently linked to the termini of carbon nanotubes.[51] The presence of the fullerene cage in complex **12** offers a new mechanism for anchoring catalytic centres utilising noncovalent interactions. Fullerenes have significant affinity for sp^2-carbon nanostructures, such as nanotubes and nanofibres, due to strong specific van der Waals forces. Indeed, titration experiments reveal that 2–3-times more of complex **12** can be loaded onto single-, double- and multiwalled carbon nanotubes compared to the non-fullerene analogue **18** (Table 7). The impact of the fullerene moiety on adhesion efficiency is even more remarkable for graphitised carbon nanofibres (GNF)—cylindrical structures with a set of step-edges formed by rolled up sheets of graphene (Figure 6)—as Cu–salen complex **18** showed no measurable adsorption on GNFs although complex **12** affinity for GNFs is comparable to that for nanotubes (Table 7).

High resolution transmission electron microscopy (HRTEM) confirms that complex **12** enters into hollow nanofibres and adsorbs on the graphitic step-edges forming

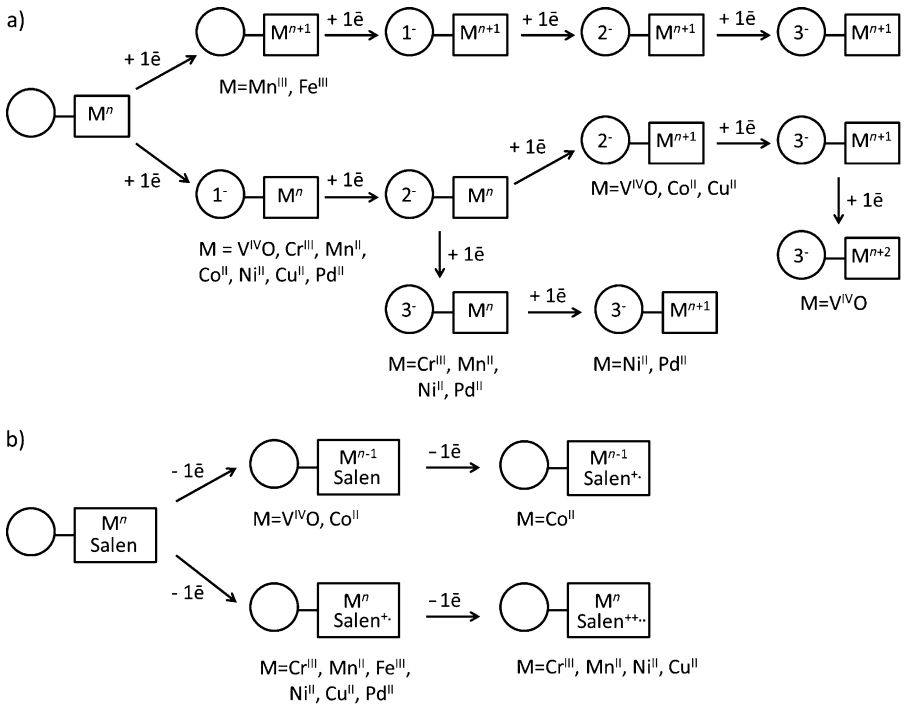

Scheme 4. Schematic representation of: a) the sequential reduction, and b) oxidation processes occurring for complexes **6**–**12** and **14**. The fullerene cage is represented as a circle and the metal–salen moiety as a rectangle, where n is the number of d-electrons on the metal centre in the neutral complex.

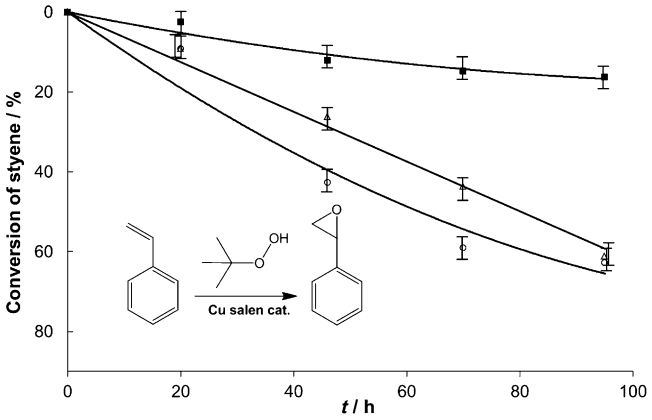

Figure 5. Reaction profiles for the oxidation of styrene with *tert*-butyl hydrogen peroxide in the presence of **12** (circles), **18** (triangles) and with no metal complex (squares).

Table 7. Adsorption data for **18** and **12** on a variety of carbon nanostructures (single- (SWNTs), double- (DWNTs), and multiwalled carbon nanotubes (MWNTs) and graphitised carbon nanofibres (GNFs)), quoted in mmol of complex per g of carbon support material and measured by UV/Vis spectroscopy in dichloromethane. Enhancement factor (last column) is the increase of affinity due to the fullerene moiety in complex **12**.

Carbon structure	Complex **18** [mmol g^{-1}]	Complex **12** [mmol g^{-1}]	Enhancement factor
SWNTs	7.644×10^{-3}	2.323×10^{-2}	3.04
DWNTs	1.496×10^{-2}	2.708×10^{-2}	1.81
MWNTs	3.280×10^{-3}	6.483×10^{-3}	1.98
GNFs	0	1.657×10^{-3}	N/A[a]

[a] Not applicable.

van der Waals contacts with GNF (Figure 6c). The fullerene part of the complex can be clearly observed in HRTEM images as a circle with diameter of approximately 0.7 nm, but imaging of the Cu–salen part is more challenging because of the limited stability of organic groups in the electron beam. Energy dispersive X-ray (EDX) spectroscopy performed for an isolated **12**@GNF structure confirms the presence of copper inside GNF (Figure 6d).

Titration and electron microscopy measurements both demonstrate that fullerene–salen complexes provide a facile route for the secure anchoring of catalytic metal centres on carbon support materials leading to a new family of hybrid nanostructures that show promise for applications in heterogeneous catalysts.

Conclusion

We have developed a five-step synthetic procedure to link fullerene C_{60} and salen units within a ligand molecule. The salen part binds a wide range of transition metals [{V(O)}^{IV}, Cr^{III}, Mn^{II}, Fe^{III}, Co^{II}, Ni^{II}, Cu^{II}, Zn^{II} and Pd^{II}] bringing them in close proximity to the fullerene cage (c.a. 6–7 Å). Kinetics studies confirm that complexation reactions are only slightly hindered by the presence of the bulky fullerene moiety when compared to fullerene-free analogues of salen. Com-

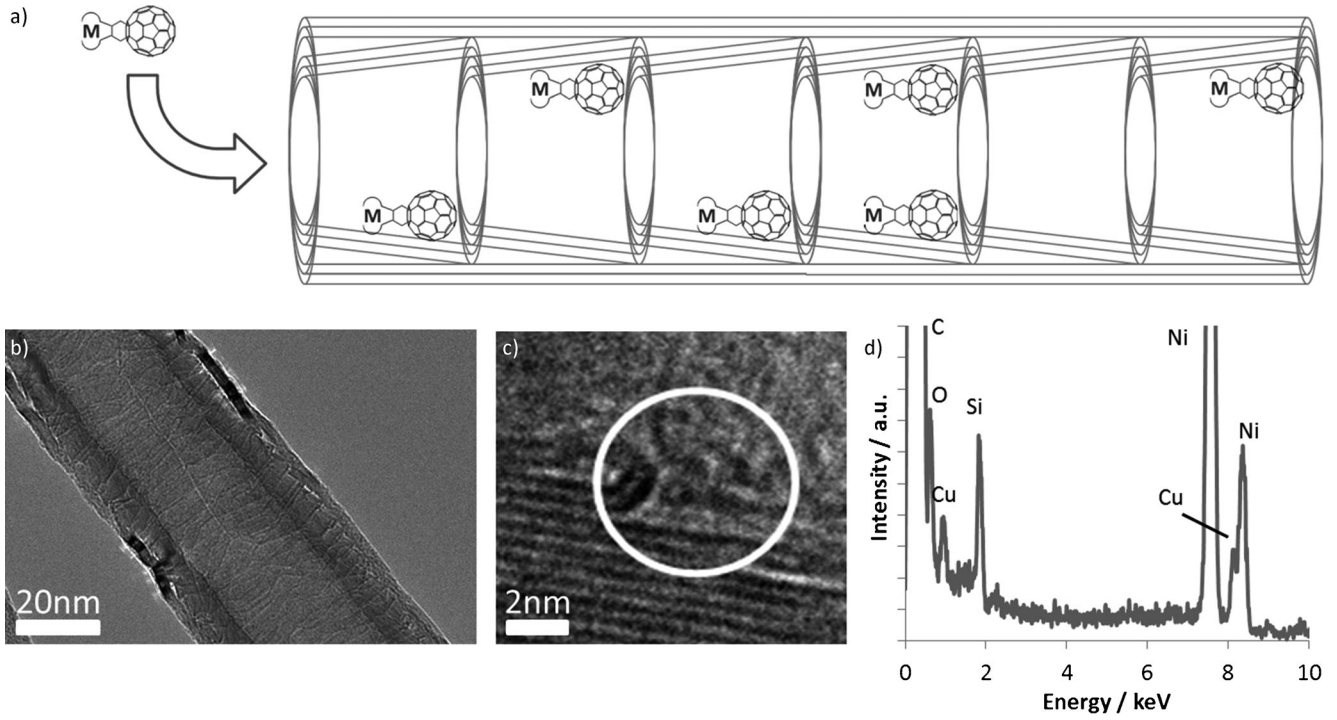

Figure 6. a) Schematic representation of complex **12** adsorbed on the step-edges in the internal channel of a graphitised carbon nanofibre. HRTEM images of the **12**@GNF composite show: b) the overall structure of the nanofibre, and c) a high-magnification image of a step-edge with adsorbed fullerene molecule (~0.7 nm circle in the centre of the white circle). d) EDX spectrum of an individual **12**@GNF structure confirming the presence of copper complex (the Ni peaks are due to the TEM specimen grid).

parison of different transition metals indicated an increase in activation energy of metal coordination following the order Cu < Ni < Co. The presence of *t*Bu groups in the ligand enhances the solubility and promotes stability of metal complexes with fullerene—two major problems that have previously thwarted the development of this type of compound.

The presence of the metal–salen group drastically affects the optical properties of the fullerene derivatives. Although the fullerene cage itself possesses only weak transitions in a limited region of the visible spectrum (~430 nm), the metal–salen group introduces strong absorptions in a wide range from 400 to 630 nm, which are determined by the nature of the transition metal. Furthermore, the presence of the metal–salen moiety enhances the redox properties of these dyad molecules by the addition of further acceptor orbitals and, more importantly, by the incorporation of readily accessible donor orbitals. The optical and redox properties of the fullerene and metal–salen moieties in these complexes remain distinct despite the close proximity of the metal centres to the fullerene cage, and thus can be exploited in molecular electronics and spintronics, photovoltaics and catalysis. The presence of the fullerene cage crucially enables the catalytically, optically and magnetically active metal–salen centres to be anchored to a variety of carbon nanostructures allowing the construction of nanoscale architectures with well-defined structure and functional properties that can be exploited in electronic devices and chemical nanoreactors.

Experimental Section

The Supporting Information contains experimental data, ^{1}H and ^{13}C NMR spectra, MALDI mass spectra, electrochemistry results, DFT geometry optimisation results, metal binding studies procedures and data processing, nanotube absorption experiments results.

Acknowledgements

We thank EPSRC, Royal Society, Nottingham Nanoscience and Nanotechnology Centre and the University of Nottingham for support. A.N.K. and E.B. acknowledge the award of ERC for Starter Grants, and M.S. acknowledges support through an ERC Advanced Grant. D.M. acknowledges receipt of funding from Marie Cure Early Training Network FUMASSEC.

[1] K. Domen, J. N. Kondo, H. Hara, T. Takata, *Bull. Chem. Soc. Jpn.* **2000**, *73*, 1307.

[2] G. Yu, J. Gao, J. Hummelen, C. F. Wudl, A. J. Heeger, *Science* **1995**, *270*, 1789.

[3] a) H. Kurreck, M. Huber, *Angew. Chem.* **1995**, *107*, 929; *Angew. Chem. Int. Ed. Engl.* **1995**, *34*, 849; b) H. A. Staab, A. Feurer, R. Hauck, *Angew. Chem.* **1994**, *106*, 2542; *Angew. Chem. Int. Ed. Engl.* **1995**, *33*, 2428; c) M. R. Roest, J. W. Verhoeven, W. Schiddeboon, M. Warman, J. M. Lawson, M. N. Paddon-Row, *J. Am. Chem. Soc.* **1996**, *118*, 1762; d) D. Gust, T. A. Moore, A. L. Moore, *Pure Appl. Chem.* **1998**, *70*, 2189; e) D. Gust, T. A. Moore, A. L. Moore, *Acc. Chem. Res.* **1993**, *26*, 198; f) M. R. Wasielewski, *Chem. Rev.* **1992**, *92*, 435; g) M. N. Paddon-Row, *Acc. Chem. Res.* **1994**, *27*, 18; h) A. J. Bard, M. A. Fox, *Acc. Chem. Res.* **1995**, *28*, 141; i) T. J. Meyer, *Acc. Chem. Res.* **1989**, *22*, 163; j) P. Piotrowiak, *Chem. Soc. Rev.* **1999**, *28*, 143; k) J. L. Delgado, P.-A. Bouit, S. Filippone, M. Á. Herranz, N. Martín, *Chem. Commun.* **2010**, *46*, 4853.

[4] A. Mateo-Alonso, D. Guldi, F. Paolucci, M. Prato, *Angew. Chem.* **2007**, *119*, 8266; *Angew. Chem. Int. Ed.* **2007**, *46*, 8120.

[5] D. González-Rodríguez, T. Torres, D. M. Guldi, J. Riviera, M. Angeles Herranz, L. Echegoyen, *J. Am. Chem. Soc.* **2004**, *126*, 6301.

[6] a) S. Plant, T. Cheong Ng, J. Warner, G. Dantelle, A. Ardavan, A. Briggs, K. Porfyrakis, *Chem. Commun.* **2009**, 4082; b) A. Tiwari, G. Dantelle, K. Porfyrakis, A. Watt, A. Ardavan, A. Briggs, *Chem. Phys. Lett.* **2008**, *466*, 155; c) J. J. L. Morton, A. Tiwari, G. Dantelle, K. Porfyrakis, A. Ardavan, G. A. D. Briggs, *Phys. Rev. Lett.* **2008**, *101*, 013002; d) P. Dunk, N. Kaiser, M. Mulet-Gas, A. Rodríguez-Fortea, J. Poblet, H. Shinohara, C. Hendrickson, A. Marshall, H. Kroto, *J. Am. Chem. Soc.* **2012**, *134*, 9380.

[7] a) C. Reed, R. Bolskar, *Chem. Rev.* **2000**, *100*, 1075; b) K. Himmel, M. Jansen, *Eur. J. Inorg. Chem.* **1998**, 1183; c) D. Konarev, R. Lyubovskaya, N. Drichko, E. Yudanova, Y. Shul′ga, A. Litvinov, V. Semkin, B. Tarasov, *J. Mater. Chem.* **2000**, *10*, 803.

[8] S. Chopin, J. Cousseau, E. Levillain, C. Rovira, J. Veciana, A. S. D. Sandanayaka, Y. Araki, O, Ito, *J. Mater. Chem.* **2006**, *16*, 112.

[9] a) M. Maruyama, J. Guo, S. Nagase, E. Nakamura, Y. Matsuo, *J. Am. Chem. Soc.* **2011**, *133*, 6890; b) Y. Matsuo, A. Iwashita, E. Nakamura, *Organometallics* **2008**, *27*, 4611.

[10] M. Meijer, G. van Klink, G. van Koten, *Coord. Chem. Rev.* **2002**, *230*, 141.

[11] a) R. Fong, D. I. Schuster, S. R. Wilson, *Org. Lett.* **1999**, *1*, 729; b) H. Imahori, H. Yamada, Y. Nishimura, I. Yamazaki, Y. Sakata, *J. Phys. Chem. B* **2000**, *104*, 2099; c) H. Imahori, H. Yamada, S. Ozawa, Y. Sakata, K. Ushida, *Chem. Commun.* **1999**, 1165; d) H. Imahori, N. Norteda, H. Yamada, Y. Nishimura, I. Yamazaki, Y. Sakata, S. Fukuzumi, *J. Am. Chem. Soc.* **2001**, *123*, 100; e) C. Luo, D. M. Guldi, H. Imahori, K. Tamaki, Y. Sakata, *J. Am. Chem. Soc.* **2000**, *122*, 6535; f) A. S. D. Sandanayaka, K. I. Ikeshita, Y. Araki, N. Kihara, Y. Furusho, T. Takata, O. Ito, *J. Mater. Chem.* **2005**, *15*, 2276; g) F. D′Souza, S. Gadde, D. M. Shafiqul Islam, C. A. Wijesinghe, A. L. Schumacher, M. E. Zandler, Y. Araki, O. Ito, *J. Phys. Chem. A* **2007**, *111*, 8552.

[12] a) T. Torres, A. Gouloumis, D. Sanchez-Garcia, J. Jayawickramarajah, W. Seitz, D. M. Guldi, J. L. Sessler, *Chem. Commun.* **2007**, 292; b) D. González-Rodríguez, T. Torres, D. M. Guldi, J. Rivera, M. A. Herranz, L. Echegoyen, *J. Am. Chem. Soc.* **2004**, *126*, 6301.

[13] a) F. Diederich, U. Jonas, V. Gramlich, A. Herrmann, H. Ringsdorf, C. Thilgen, *Helv. Chim. Acta* **1993**, *76*, 2445; b) J. Osterodt, A. Zett, F. Vögtle, *Tetrahedron* **1996**, *52*, 4949; c) S. R. Wilson, Y. Wu, *J. Chem. Soc. Chem. Commun.* **1993**, 784.

[14] a) J. Fan, T. W. Chamberlain, Y. Wang, S. H. Yang, A. J. Blake, M. Schröder, A. N. Khlobystov, *Chem. Commun.* **2011**, *47*, 5696; b) C. Du, Y. Li, S. Wang, Z. Shi, S. Xiao, D. Zhu, *Synth. Methods* **2001**, *124*, 287.

[15] Y. Rio, D. Sánchez-García, W. Seitz, T. Torres, J. L. Sessler, D. M. Guldi, *Chem. Eur. J.* **2009**, *15*, 3956.

[16] J. Fan, Y. Wang, A. J. Blake, C. Wilson, E. S. Davies, A. N. Khlobystov, M. Schröder, *Angew. Chem.* **2007**, *119*, 8159; *Angew. Chem. Int. Ed.* **2007**, *46*, 8013.

[17] a) E. N. Jacobsen, in *Comprehensive Organometallic Chemistry II, Vol. 12* (Eds.: E. W. Abel, F. G. A. Stone, G. Wilkinson), Pergamon, New York, **1995**, p. 1097; b) T. Katsuki, *Coord. Chem. Rev.* **1995**, *140*, 189; c) L. Canali, D. C. Sherrington, *Chem. Soc. Rev.* **1999**, *28*, 85; d) E. N. Jacobsen, *Acc. Chem. Res.* **2000**, *33*, 421; e) D. A. Atwood, M. J. Harvey, *Chem. Rev.* **2001**, *101*, 37; f) T. Katsuki, *Synlett* **2003**, 281; g) P. G. Cozzi, *Chem. Soc. Rev.* **2004**, *33*, 410; h) T. Katsuki, *Chem. Soc. Rev.* **2004**, *33*, 437; i) J. F. Farlow, E. N. Jacobsen, *Top. Organomet. Chem.* **2004**, *7*, 123; j) E. M. McGarrigle, D. G. Gilheany, *Chem. Rev.* **2005**, *105*, 1563.

[18] E. Kimura, S. Aoki, T. Koike, M. Shiro, *J. Am. Chem. Soc.* **1997**, *119*, 3068.

[19] P. Belik, A. Gügel, A. Kraus, M. Walter, K. Müllen, *J. Org. Chem.* **1995**, *60*, 3307.
[20] J. R. Deye, A. N. Shiveley, S. M. Goins, L. Rizzo, S. A. Oehrle, K. A. Walters, *Inorg. Chem.* **2008**, *47*, 23.
[21] a) J. Wöltinger, J.-E. Bäckvall, Á. Zsigmond, *Chem. Eur. J.* **1999**, *5*, 1460; b) M. Franks, A. Gadzhieva, L. Ghandhi, D. Murrell, A. J. Blake, E. S. Davies, W. Lewis, F. Moro, J. McMaster, M. Schröder, *Inorg. Chem.* **2013**, *52*, 660.
[22] L. Ding, Z. Chu, L. Chen, X. Lü, B. Yan, J. Song, D. Fan, F. Bao, *Inorg. Chem. Commun.* **2011**, *14*, 573.
[23] N. Meyer, P. Roesky, *Z. Anorg. Allg. Chem.* **2007**, *633*, 2292.
[24] M. Belmonte, S. Wezenberg, R. Haak, D. Anselmo, E. Escudero-Adán, J. Benet-Buchholz, A. Kleij, *Dalton Trans.* **2010**, *39*, 4541.
[25] M. Nomura, T. Yamaguchi, *J. Phys.* **1986**, *47*, 619.
[26] J. van Niekerk, F. Schoening, *Acta Crystallogr.* **1953**, *6*, 609.
[27] C. Hendriks, H. van Beek, P. Heertjes, *Ind. Eng. Chem. Prod. Res. Dev.* **1979**, *18*, 43.
[28] A. Skapski, M. Smart, *Chem. Commun.* **1970**, 658.
[29] Y. Shimazaki, T. Yajima, F. Tani, S. Karasawa, K. Fukui, Y. Naruta, O. Yamauchi, *J. Am. Chem. Soc.* **2007**, *129*, 2559.
[30] A. Hirsch, T. Grösser, A. Siebe, A. Soi, *Chem. Ber.* **1993**, *126*, 1061.
[31] A. Pui, C. Policar, J.-P. Mahy, *Inorg. Chim. Acta* **2007**, *360*, 2139.
[32] M. Carter, P. Rillema, F. Basolo, *J. Am. Chem. Soc.* **1974**, *96*, 392.
[33] S. Biswas, A. Dutta, K. Mitra, M.-C. Dul, S. Dutta, R. Lucas, B. Adhikary, *Inorg. Chim. Acta* **2011**, *377*, 56.
[34] M. Weberski, C. McLauchlan, C. Hamaker, *Polyhedron* **2006**, *25*, 119.
[35] R. Klement, F. Stock, H. Elias, H. Paulus, P. Pelikán, M. Valko, M. Mazúr, *Polyhedron* **1999**, *18*, 3617.
[36] N. Youssef, E. El-Zahany, B. Barsoum, A. El-Seidy, *Transition Met. Chem.* **2009**, *34*, 905.
[37] S. Alghool, H. El-Halim, A. Dahshan, *J. Mol. Struct.* **2010**, *983*, 32.
[38] E. Pas, A. Kilic, M. Durgun, I. Yilmaz, I. Ozdemir, N. Gurbuz, *J. Organomet. Chem.* **2009**, *694*, 446.
[39] L. Echegoyen, L. E. Echegoyen, *Acc. Chem. Res.* **1998**, *31*, 593.
[40] S. Vail, P. Krawczuk, D. Guldi, A. Palkar, L. Echegoyen, J. Tomé, M. Fazio, D. Schuster, *Chem. Eur. J.* **2005**, *11*, 3375.
[41] F. Thomas, O. Jarjayes, C. Duboc, C. Philouze, E. Saint-Aman, J.-L. Pierre, *Dalton Trans.* **2004**, 2662.
[42] O. Rotthaus, O. Jarjayes, F. Thomas, C. Philouze, E. Saint-Aman, J.-L. Pierre, *Dalton Trans.* **2007**, 889.
[43] Q. Xie, F. Arias, L. Echegoyen, *J. Am. Chem. Soc.* **1993**, *115*, 9818.
[44] a) L. Bogani, W. Wernsdorfer, *Nat. Mater.* **2008**, *7*, 179; b) W. Y. Kim, K. S. Kim, *Acc. Chem. Res.* **2010**, *43*, 111.
[45] a) F. Hueso-Urena, N. A. Illan-Cabeza, M. N. Moreno-Carretero, J. M. Martinez-Martos, M. J. Ramirez-Exposito, *J. Inorg. Biochem.* **2003**, *94*, 326; b) F. Farzaneh, M. Majidian, M. Ghandi, *J. Mol. Catal. A* **1999**, *148*, 227; c) G. T. Musie, M. Wei, B. Subramaniam, D. H. Busch, *Inorg. Chem.* **2001**, *40*, 3336.
[46] a) M. Tokunaga, J. F. Larrow, F. Kakiuchi, E. N. Jacobson, *Science* **1997**, *277*, 936; b) M. D. Angelino, P. E. Laibinis, *J. Polym. Sci. Part A* **1999**, *37*, 3888.
[47] a) C. Chapuis, D. Jacoby, *Appl. Catal. A* **2001**, *221*, 93; b) L. Liu, M. Rozenman, R. Breslow, *Bioorg. Med. Chem.* **2002**, *10*, 3973; c) H. Hayashi, *J. Biochem.* **1995**, *118*, 463.
[48] a) H. Yoon, T. R. Wagler, K. J. O'Connor, C. J. Burrows, *J. Am. Chem. Soc.* **1990**, *112*, 4568; b) J. F. Kinneary, J. S. Albert, C. J. Burrows, *J. Am. Chem. Soc.* **1988**, *110*, 6124; c) H. Yoon, C. J. Burrows, *J. Am. Chem. Soc.* **1988**, *110*, 4087; d) V. Ayala, A. Corma, M. Iglesias, J. A. Rincón, F. Sánchez, *J. Catal.* **2004**, *224*, 170; e) M. R. Maurya, S. J. J. Titinchi, S. Chand, *J. Mol. Catal. A* **2003**, *201*, 119; f) D. Chatterjee, S. Mukherjee, A. Mitra, *J. Mol. Catal. A* **2000**, *154*, 5.
[49] E. N. Jacobsen, in *Catalytic Asymmetric Synthesis* (Ed.: I. Ojima), VCH, Weinheim, **1993**, Chapter 42.
[50] C. Jin, Y. J. Jia, B. B. Fan, J. H. Ma, R. F. Li, *Chin. Chem. Lett.* **2006**, *17*, 419.
[51] C. Baleizao, B. Gigantea, H. Garciab, A. Cormab, *J. Catal.* **2004**, *221*, 77.

Received: March 6, 2013
Published online: July 23, 2013

